

# Climate signatures on lake and wetland size distributions in arctic deltas

Lawrence Vulis<sup>1\*</sup>, Alejandro Tejedor<sup>2,1</sup>, Ilya Zaliapin<sup>3</sup>, Joel C. Rowland<sup>4</sup>, and  
Efi Foufoula-Georgiou<sup>1,5</sup>

<sup>1</sup>Department of Civil and Environmental Engineering, University of California Irvine, [lvulis@uci.edu](mailto:lvulis@uci.edu)

<sup>2</sup>Department of Science and Engineering, Sorbonne University Abu Dhabi

<sup>3</sup>Department of Mathematics and Statistics, University of Nevada Reno

<sup>4</sup>Earth and Environmental Sciences Division, Los Alamos National Laboratory

<sup>5</sup>Department of Earth System Science, University of California Irvine

## Key Points:

1. Lake areas in arctic deltas exhibit a lognormal distribution associated with a simple mechanistic growth process.
2. Wetland areas exhibit a power law distribution consistent with inundated fractal topography.
3. Colder arctic deltas have larger average lake sizes, likely due to thicker permafrost restricting sub-lake hydrologic connectivity.

## ABSTRACT

Understanding how thermokarst lakes on arctic river deltas will respond to rapid warming is critical for projecting how carbon storage and fluxes will change in those vulnerable environments. Yet, this understanding is currently limited partly due to the complexity of disentangling significant interannual variability from the longer-term surface water signatures on the landscape, using the summertime window of optical spaceborne observations. Here, we rigorously separate perennial lakes from ephemeral wetlands on 12 arctic deltas and report distinct size distributions and climate trends for the two waterbodies. Namely, we find a lognormal distribution for lakes and a power-law distribution for wetlands, consistent with a simple proportionate growth model and inundated fractal topography, respectively. Furthermore, while no trend with temperature is found for wetlands, a statistically significant decreasing trend of mean lake size with warmer temperatures is found, attributed to colder deltas having deeper and thicker permafrost preserving larger lakes.

## Plain Language Summary

Arctic river deltas are landscapes facing significant risk from climate change, in part due to their unique permafrost features. In particular, thermokarst lakes in ice-rich permafrost are expected to both expand and drain under warming-induced permafrost thaw, reconfiguring deltaic hydrology and impacting the arctic carbon cycle. A limitation in understanding how thermokarst lake cover might be changing, is the significant interannual variability in water cover in flat regions such as deltas, which makes it difficult to distinguish between perennially inundated, thermally relevant waterbodies, and ephemerally inundated waterbodies. Here, we present a pan-Arctic study of 12 arctic deltas wherein we classify observed waterbodies into perennial lakes and ephemeral wetlands capitalizing on the historical record of remote sensing data. We provide evidence that thermokarst lake sizes are universally lognormally distributed and that historical temperature trends are encoded in lake sizes, while wetland sizes are power law distributed and have no temperature trend. These findings pave the way for quantitative insight into lake cover changes on arctic deltas and associated carbon and hydrologic cycle impacts under future climate change.

## 43 1. Introduction

44 Coastal river deltas are landscapes at significant risk from sea level rise and sediment  
45 deprivation (Nienhuis et al., 2020; Syvitski et al., 2009). Arctic deltas are likely more vulnerable  
46 than their temperate counterparts due to the presence of thermokarst lakes in permafrost, which  
47 are sensitive to rapid Arctic warming (Emmerton et al., 2007; Piliouras & Rowland, 2020; Walker,  
48 1998). Pan-arctic thermokarst lake coverage is responding to warmer temperatures in complex  
49 ways, as temperature-driven ground ice loss drives lake growth via retrogressive thaw slumping  
50 along lake shorelines (Grosse et al., 2013) but also generates surface and sub-surface hydrologic  
51 connectivity that can cause lake drainage (Grosse et al., 2013; Jones et al., 2020; Rowland et al.,  
52 2011; Yoshikawa & Hinzman, 2003). Observed changes in lake area over the last 50 years have  
53 shown both positive and negative trends depending on local hydrology, climate, permafrost  
54 zonation, ice content, landscape age, and geomorphic setting (Arp et al., 2011; Chen et al., 2012;  
55 Jones et al., 2011; Nitze et al., 2018; Plug et al., 2008; Smith et al., 2005). Irrespective of whether  
56 lake coverage is expanding or decreasing, change is expected to have consequences for the  
57 permafrost carbon cycle, as thermokarst lake expansion accelerates permafrost thaw and expedites  
58 the release of previously frozen carbon into the atmosphere as methane and CO<sub>2</sub>, while lake  
59 drainage may slow permafrost-thaw and associated carbon emissions (van Huissteden et al., 2011).  
60 Major arctic deltas store approximately  $91 \pm 39$  Pg-Carbon, potentially making them significant  
61 sources of future carbon emissions (Schuur et al., 2015). Moreover, thermokarst lakes in deltas  
62 modulate transport of riverine freshwater, sediment, and nutrient fluxes to the Arctic ocean, by  
63 trapping and holding sediment (Marsh et al., 1999; Piliouras & Rowland, 2020) and modifying the  
64 residence times and pathways of nutrient transport through the delta (Lesack & Marsh, 2010;  
65 Squires et al., 2009; Tank et al., 2009). Therefore, changing deltaic lake coverage and its spatial

66 distribution will also alter the timing and magnitudes of riverine fluxes to the Arctic Ocean, which  
67 has broader implications for near-shore circulation and ecosystem productivity (Lique et al., 2016).

68 We hypothesize that lake size variability and spatial arrangement across arctic deltas (Figure  
69 1) may encode information on climate influence in permafrost environments, akin to how channel  
70 network structure is a signature of the riverine, tidal, and fluvial fluxes which shape temperate  
71 deltas (Nienhuis et al., 2016, 2018; Tejedor et al., 2015b, 2015a, 2016, 2017). In particular, we  
72 hypothesize that two primary drivers of lake size variability across deltas are ice content and  
73 climate and test this hypothesis quantitatively. Physically we expect that colder deltas have thicker  
74 permafrost which is able to support larger lakes, by preventing connection to the sub-permafrost  
75 groundwater table that can lead to eventual lake drainage (Grosse et al., 2013; Walvoord &  
76 Kurylyk, 2016; Yoshikawa & Hinzman, 2003) or diminished lake growth rates. We also expect  
77 that deltas with greater soil ice fraction will have larger lakes as soil ice acts as a subsurface  
78 hydraulic barrier, while soil ice melt induces subsidence and therefore lake growth. Discovering  
79 and quantifying data-driven relationships between lake size and ice content or temperature will be  
80 useful for constraining physical models and predicting future arctic delta morphology in a warmer  
81 climate.

82 However, a challenge in assessing the climatic signature on thermokarst lake sizes is the  
83 significant interannual (Grosse et al., 2013; Rey et al., 2019) and seasonal variability (Chen et al.,  
84 2012, 2013; Cooley et al., 2019; Vulis et al., 2020) in lake area which makes it difficult to  
85 distinguish perennial waterbodies (lakes) from ephemerally inundated depressions (wetlands)  
86 using the short summertime window of available spaceborne observations. In particular, seasonal  
87 water may inundate ephemeral wetlands, which would be misidentified as perennially inundated  
88 lakes from remote sensing imagery. The processes underlying ephemeral wetland versus perennial

89 lake formation are distinct, as lakes are the result of thermokarst-driven growth and evolution  
90 (Grosse et al., 2013), while wetlands are the result of hydrologic variability, and as defined in this  
91 study only seasonally inundated (Le & Kumar, 2014). Mixing of the two waterbodies is certain to  
92 hide causative patterns and signatures, as lakes and wetlands have different time scales of thermal  
93 impact on the landscape, and are thus expected to show different expressions of their size  
94 distribution and their dependence on climate.

## 95 **2. Study sites, data, and lake and wetland extraction**

96 Lake and wetland size distributions on 12 arctic deltas characterized by a range of air  
97 temperature and ice content across Siberia (Indigirka, Kolyma, Lena, Nadym, Ob, Pur, Yana, and  
98 Yenisei), Canada (Mackenzie), and Alaska (Colville, Kobuk, and Yukon) were examined (Figure  
99 1). The deltas include those formed by the six arctic rivers with the greatest discharge and other  
100 major rivers along the Siberian and Alaskan coastlines. Lakes and wetlands were extracted over  
101 the subaerial portion of each delta, which was delineated using Google Earth. Delta Mean Annual  
102 Air Temperature (MAAT) was obtained from 2000-2016 using the 15-km spatial resolution Arctic  
103 Systems Reanalysis V2 (Bromwich et al., 2017). Delta soil ice content was estimated from a 12.5-  
104 km spatial resolution ice classification map (Brown et al., 1997).

105 To distinguish between hydrologically perennial lakes and ephemeral wetlands, we utilized the  
106 spatiotemporal interannual variability of water coverage over each delta from 1999 to 2018. We  
107 used the Landsat-derived, 30-m spatial resolution Global Surface Water (GSW) dataset which  
108 provides monthly-composited water masks from March 1984 to December 2018 that classify the  
109 landscape into 30-m pixels that are land, water, or no data (i.e. unable to classify due to cloud  
110 cover, Landsat-7 striping, or snow and ice cover) (Pekel et al., 2016). Due to sparse data  
111 availability prior to 1999 on most deltas, we only analyzed the period from 1999 to 2018, and to

112 remove the effect of significant snowmelt and spring time flooding we only analyzed July water  
113 masks, similar to other studies (Muster et al., 2019; Nitze et al., 2018). We only examined the  
114 subaerial portion of each delta, manually delineated using Google Earth.

115 To identify and separate lakes from wetlands, we first computed for every pixel  $i$  the July  
116 “water pixel occurrence”,  $w_i$ , as the fraction of Julys from 1999 to 2018 for which the pixel was  
117 classified as water, discarding no-data pixels (Figure 2a). The water pixel occurrence  $w_i$  can take  
118 values from 0 to 1, with  $w_i = 1$  if and only if the pixel was classified as water for the whole record  
119 and  $w_i = 0$  if and only if the pixel was classified as land for the whole record. Second, we  
120 identified a reference year,  $y^*$ , with water coverage on the subaerial delta closest to that of the  
121 temporal average over the 20-year period of record and sufficient data quality, i.e. greater than  
122 99% pixels classified as land or water and no significant geo-referencing (collocation) errors, and  
123 used this year to identify individual waterbodies using 8-neighbor connected component analysis  
124 (see Supplementary Material, Figures S1 to S3 for details on selection of  $y^*$ ). Third, we classified  
125 the waterbodies identified in year  $y^*$  into lakes and wetlands using the water pixel occurrence,  $w_i$ .  
126 For each waterbody,  $O_k^{y^*}$ , we computed the “occurrence index”  $B_k$  as the mean of  $w_i$  for all pixels  
127  $i$  within  $O_k^{y^*}$ , which corresponds to the fraction of pixels within the waterbody that were on average  
128 occupied by water over the 20 years (Julys) of record. A waterbody was then classified as a lake  
129 if  $B_k$  exceeded a threshold value  $\theta$  and as a wetland if  $B_k$  was less than  $\theta$ . We evaluated the results  
130 over a range of  $\theta$  values, from  $\theta = 0.80$  to  $\theta = 0.90$ , to account for differences in the flooding  
131 regime across different deltas and to test the robustness of our results (Tables S1 to S3, Figures S4  
132 and S5). The lake and wetland size distributions shown in Figures 3 and 4 are extracted at a  
133 threshold value of  $\theta = 0.85$ . Only waterbodies at least  $5,400 \text{ m}^2$  (i.e. 6 pixels) in size were included  
134 in our analysis to reduce estimation errors at small areas. We tested the robustness of our

135 methodology by performing a duplication, wherein we selected an alternative reference year,  $y_{alt}^*$ ,  
136 with similar water coverage and data quality to extract waterbody extents and repeated the analysis  
137 (Supplementary Material, Table S4, and Figures S4 and S5). All analyses were performed in R  
138 using geospatial and image processing packages (Gillespie, 2015; Hijmans, 2020; Pau et al., 2010;  
139 Pebesma, 2018, 2020).

### 140 **3. Lake size distributions and a proportionate growth model**

141 From a simple thermodynamical perspective, thermokarst lakes are thermal reservoirs, which  
142 interact with their surroundings via heat exchange. In particular, unfrozen lake waters are net heat  
143 sources, thawing the surrounding ice-rich soil which leads to lake basin expansion (Grosse et al.,  
144 2013). As larger lakes have a larger thermal inertia, they remain unfrozen for longer periods  
145 (Grosse et al., 2013) and maintain larger lake to soil temperature gradients, which enables them to  
146 grow at faster rates. Thus, based on this simple thermodynamical argument, and on field  
147 observations (Jones et al., 2011), we can postulate that thermokarst lake growth is compatible with  
148 a stochastic proportionate growth model (Crow & Shimizu, 1988; Mitzenmacher, 2004) (i.e.  
149 growth rate proportional to lake size), where stochasticity arises from the variability of soil  
150 properties which modulate growth. A key property of this general class of proportionate growth  
151 models is that they generate objects (in our case lakes) with sizes obeying a lognormal (LN)  
152 distribution (Supplementary Material) (Crow & Shimizu, 1988). Thus, our expectation based on  
153 simple physical arguments is that arctic deltas should universally exhibit lakes whose sizes are  
154 lognormally distributed. In particular, since we only observe lake sizes above 5,400 m<sup>2</sup> (6 pixels)  
155 we expect lake sizes to follow a truncated lognormal distribution (Equation 1):

$$f_x(x; \nu, \beta^2) = \begin{cases} 0 & \text{for } x < x_{min} \\ \frac{1}{x\beta\sqrt{2\pi}} e^{-\frac{(\ln(x)-\nu)^2}{2\beta^2}} & \text{for } x \geq x_{min} \\ \left[1 - \Phi\left(\frac{\ln(x_{min})-\nu}{\beta}\right)\right] & \end{cases}, \quad (1)$$

157 where  $\Phi(\cdot)$  is the cumulative distribution function (CDF) of a standard normal variable,  $\nu$  is the  
 158 scale parameter,  $\beta$  the shape parameter, and  $x_{min}$  the minimum value at which the LN is observed,  
 159 here 5,400 m<sup>2</sup> (Clauset et al., 2009). When  $x_{min}$  approaches zero, the denominator approaches  
 160 unity and Equation (1) is simply the LN distribution.

161 Having separated lakes and wetlands based on the methodology outlined in section 2, we  
 162 examined the empirical probability density function (PDF) of lake sizes (Figure 3a). As postulated,  
 163 we found that the examined lake sizes can be accurately described by a truncated LN distribution  
 164 for the whole range of lake sizes (spanning 3.5 orders of magnitude) in the 12 deltas under study  
 165 (see Quantile-Quantile (Q-Q) plots in Figure 3b). The rigorous Lilliefors-corrected Kolmogorov-  
 166 Smirnov (KS) test (Clauset et al., 2009), shows that for every delta, the fitted LN distribution could  
 167 not be rejected at the 5% significance level within the range of thresholds  $\theta$  utilized for the  
 168 identification of lakes from the general waterbody population (Tables S1 to S3). For most deltas,  
 169 the LN fit could not be rejected over the entire range, but in several deltas the test outcome  
 170 depended on the threshold, due to the fact that the hydrogeomorphological specificities of the  
 171 different deltas can lead to potential suboptimal lake/wetland separation for certain threshold  
 172 values and ranges of waterbody sizes. Furthermore, the robustness of the revealed universality of  
 173 the LN distribution of lake sizes was confirmed by successfully testing that lake sizes are LN  
 174 distributed when alternative years were used as reference to extract waterbodies (Table S4, Figure  
 175 S4). Previous empirical (suggesting different distributions for arctic waterbodies) (Muster et al.,  
 176 2019) and theoretical (suggesting a proportionate growth model) (Victorov et al., 2019) studies  
 177 have failed to demonstrate this universality because thermokarst lakes and wetlands were analyzed

178 together (Table S5 and Figure S6), and as we show in the next section wetlands do exhibit a  
179 different distribution.

#### 180 **4. Wetland size distributions and an inundated topography model**

181 Arctic delta wetlands are, by definition, ephemeral waterbodies emerging on the delta top due  
182 to local ice/snow melt and riverine flooding. Therefore, wetland sizes are expected to be highly  
183 dependent on the seasonal delta hydrology, which controls overall delta wetness (hydrologic  
184 forcing), and delta topography; the topography in turn constitutes the spatial layout for inundation,  
185 and controls both the emergence of disjoint wetlands and their sizes for a given forcing. The  
186 prevalence of power-law distributions describing the sizes of waterbodies emerging from  
187 landscape inundation has been extensively documented (Bertassello et al., 2018; Cael & Seekell,  
188 2016; Le & Kumar, 2014; Mandelbrot, 1982). For instance, recent analysis of the sizes of  
189 waterbodies identified from inundating low-relief topography and observed wetlands in the  
190 contiguous United States were found to exhibit power law distribution of areas consistent with  
191 inundated fractal topography (Bertassello et al., 2018; Le & Kumar, 2014). Therefore, our  
192 hypothesis was that the Arctic delta wetlands will follow a similar distribution. The form of the  
193 power law PDF used in this study is given in Equation (2), where  $x_0$  is the minimum size above  
194 which the power law is fit and  $\alpha$  is the power law exponent (Clauset et al., 2009):

$$195 \quad f_X(x; \alpha) = \frac{\alpha-1}{x_0} \left(\frac{x}{x_0}\right)^{-\alpha}, x > x_0 \quad (2)$$

196 We observed that wetland size distributions in the 12 arctic deltas indeed show strong evidence  
197 of being power law distributed (log-log linearity over two orders of magnitude in Figure 3c). Using  
198 the robust methodology of Clauset et al. (2009) for power law testing and fitting, we found that  
199 the power-law hypothesis for wetland sizes could not be rejected at the 5% significance level with

200 a Lilliefors-corrected KS test for all 12 deltas (Tables S1 to S3). As with lakes, the power law  
201 distribution of wetland sizes is robust with respect to the threshold  $\theta$ , which establishes the  
202 separation of waterbodies into lakes and wetlands (Tables S1 to S3). Moreover, the robustness of  
203 our hypothesis was verified by extracting waterbodies and identifying wetlands in an alternative  
204 reference year, wherein again most deltas displayed power law wetland size distributions (Table  
205 S4, Figure S4).

206 Recent literature has hypothesized that lakes in the Arctic are consistent with landscape  
207 inundation mechanisms (Muster et al., 2019). This hypothesis was grounded on the finding that  
208 empirical statistics of waterbodies obey two relationships (a linear relationship between  
209 conditional mean and conditional variance and a hyperbolic relationship between conditional mean  
210 and conditional skewness) which are consistent with those arising from an inundation model  
211 experiment (Muster et al., 2019). However, as we show here (Supplementary Material, Figure S8)  
212 these same relationships arise from a proportionate growth model and a LN distribution, cautioning  
213 their use for distinguishing between the power-law and LN probability distributions and making  
214 physical inferences.

## 215 **5. Climate trends**

216 How will the Arctic look like in a warmer future is a question of interest due to the critical  
217 impacts that changes in lake and wetland coverage will have on methane emissions (Engram et al.,  
218 2020; van Huissteden et al., 2011; Petrescu et al., 2010), release of old carbon (Grosse et al., 2013;  
219 Rowland et al., 2010), re-plumbing of surface-subsurface hydrologic partitioning (Walvoord &  
220 Kurylyk, 2016), and changes in water and biogeochemical cycling to the ocean (Piliouras et al.,  
221 2021; Piliouras & Rowland, 2020). Although physical models could be used to project such  
222 changes, their complexity and uncertainty in parameterizations makes it difficult to implement

223 them over large areal extents and long periods of time (van Huissteden et al., 2011; Kessler et al.,  
224 2012; Plug & West, 2009). We posit that if robust relationships between lake size distributions and  
225 climate variables can be established based on analysis of deltas across a gradient of temperature,  
226 soil ice content and permafrost coverage, valuable quantitative insight can be gained for the future.  
227 More specifically, we pose the hypothesis that lake sizes encode the signature of climate while  
228 ephemeral wetlands are mostly agnostic to it.

229 We have tested this hypothesis by analyzing the relationships between mean lake and wetland  
230 size (areal extent) with respect to MAAT and soil ice content. The data suggest that the mean  
231 thermokarst lake size increases by  $9 \cdot 10^4 \text{ m}^2$ , i.e. doubling, over a  $12^\circ\text{C}$  decrease in the average  
232 2000 to 2016 MAAT (Bromwich et al., 2017), indicating that colder deltas have significantly larger  
233 lakes on average (Figure 4a). Modern MAAT may not be representative of paleoclimatic  
234 temperature variability; however mean lake size also has a significant linear relationship ( $p =$   
235  $0.028$ ,  $R^2 = 0.40$ ) with delta apex latitude, which is a reasonable proxy for historical temperature  
236 differences between the deltas, strongly supporting a temperature to lake size relationship. Mean  
237 lake size also generally positively relates to soil ice content, as higher ice content on the delta may  
238 support lake growth due to greater settlement from ice melt (Grosse et al., 2013), with lower ice  
239 content associated with smaller lakes (Figure 4a). A similar trend between lake sizes and MAAT  
240 is observed when an alternative reference year is used to extract waterbodies in (Figure S5a),  
241 supporting the robustness of this dependence. On the other hand, the data show no relationship  
242 between mean wetland size and MAAT (Figures 4b, Figure S5b). Also expected, but confirmed,  
243 mixing the two waterbodies makes it hard to detect the climatic signal on the landscape. Indeed, a  
244 joint analysis reveals a non-significant relationship with MAAT (Figure S6d).

245 The observed relationship for mean lake size and MAAT is attributed to the greater capacity  
246 of colder deltas to support large lakes due to their presumably thicker and cooler permafrost, which  
247 prevents sub-lake taliks from connecting to the sub-permafrost groundwater table (Walvoord &  
248 Kurylyk, 2016). This connection in low relief deltaic environments would reduce lake level as  
249 river stage recedes through the summer, transitioning the margins of perennially inundated lakes  
250 to ephemerally inundated, thereby reducing lateral thermal fluxes from the lake to the surrounding  
251 permafrost, i.e. diminishing lake growth and decreasing the observed size of perennially inundated  
252 lakes (Figures 4c and 4d). Such an effect would be clearest in large lakes which have deep taliks  
253 (Grosse et al., 2013), and indeed, we found that the peripheries of large lakes were inundated more  
254 often on average over the period of record on warmer deltas compared with colder deltas (Figure  
255 4e). Note that the fraction of the periphery that remains water (inundated) on average over the  
256 period of record (Figure 4e) is computed as the average  $w_i$  of all pixels bordering the lake (in an  
257 8-neighbor sense), and then the average of large lakes (defined as those with areas between  $10^5$   
258 and  $10^6$  m<sup>2</sup>) over the entire delta computed to obtain a representative value.

259 Such a relationship may also occur due to evapotranspiration rates being higher on warmer  
260 deltas, which lead to greater lake margin loss. However, we found that average June-July  
261 precipitation minus evapotranspiration (P-ET, i.e. the vertical hydrologic budget) (Bromwich et  
262 al., 2017) over the delta is uncorrelated with MAAT, and therefore P-ET does not explain the  
263 relationship between delta temperature and how often lake peripheries are inundated (Figure S5d).  
264 This mechanism could be validated in future studies by imaging subsurface permafrost structure  
265 across the deltas which has been done in other permafrost environments (Rey et al., 2019).

266

267

## 268 **6. Perspectives and Conclusions**

269 By harnessing more than 20 years of remote sensing data over the Arctic, we have developed  
270 a methodology to classify waterbodies, depending on their year-to-year variability, as lakes  
271 (perennial) and wetlands (ephemeral). The statistical distributions of lake and wetland sizes are  
272 distinct and appear to be universal across arctic deltas, reflecting the respective underlying  
273 mechanisms driving the formation and evolution of those waterbodies. Specifically, it was found  
274 that thermokarst lake sizes obey a lognormal distribution, which can be interpreted as the emergent  
275 signature of the thermal mechanism driving lake formation and growth. On the other hand, wetland  
276 sizes were found to exhibit a power law distribution compatible with landscape inundation models  
277 relevant to ephemeral waterbodies (Bertassello et al., 2018; Le & Kumar, 2014). The difference  
278 between the underlying forming mechanisms leads also to different expectations with respect to  
279 possible relationships with climatic variables. Indeed, our results reveal a significant trend between  
280 mean lake size and mean annual air temperature, supporting the hypothesis that colder  
281 environments are able to grow and sustain larger thermokarst lakes, while no signature of climate  
282 is found in the mean wetland sizes. The power law exponents of the wetland size distributions  
283 were found to range between 1.8 and 2.8 (a smaller exponent indicates a thicker tail of the PDF)  
284 and further analysis of high-resolution topography is expected to provide additional insight on this  
285 range. The decreasing trend of mean lake size with warmer temperatures found here can form the  
286 basis for future lake area change projections, recognizing however that the relationship from the  
287 12 examined deltas, although statistically significant, explains only 40% of the variance and lake  
288 change may display significant spatial variability (Chen et al., 2012). Spatially resolved permafrost  
289 depth and ground ice content on the deltas (Rey et al., 2019), as well as analysis of physically-  
290 based models forced with different climate scenarios (Coon et al., 2019; Overeem et al., 2018) is

291 needed to better understand cause-and-effect and derive relationships that can serve as the basis of  
292 projections of landscape change (e.g. increased water ephemerality under warming scenarios) and  
293 associated carbon cycle impacts in specific delta environments.

#### 294 **Acknowledgements**

295 L.V. was supported under the NASA Earth and Space Science Fellowship Program Grant  
296 80NSSC18K1409 and the UC-National Lab In-Residence Graduate Fellowship Grant  
297 L21GF3569. E.F-G., A.T., and L.V. received support from NSF Earth Sciences Directorate Grant  
298 EAR-1811909 and the UK Research and Innovation Global Challenges Research Fund Living  
299 Deltas Hub Grant NES0089261. I.Z. received support from NSF Earth Sciences Directorate Grant  
300 EAR-1723033. J.C.R. received support as part of the Interdisciplinary Research for Arctic Coastal  
301 Environments (InterFACE) project through the Department of Energy, Office of Science,  
302 Biological and Environmental Research (BER) Regional and Global Model Analysis (RGMA)  
303 program. We thank the Luca de Felice from the Global Surface Water team for his assistance in  
304 addressing geo-referencing and pyramiding issues in the monthly water masks.

#### 305 **Data Availability**

306 The Global Surface Water monthly water masks are available via Google Earth Engine  
307 (<https://earthengine.google.com/>). The Arctic Systems Reanalysis V2 data is available from  
308 University Corporation for Atmospheric Research (UCAR) Research Data Archive (RDA)  
309 (<https://rda.ucar.edu/datasets/ds631.1/>). The ice content data is available from the National Snow  
310 and Ice Data Center (NSIDC) (<https://nsidc.org/data/ggd318>). Code to reproduce this analysis are  
311 available from the corresponding author upon request.

312

313 **References**

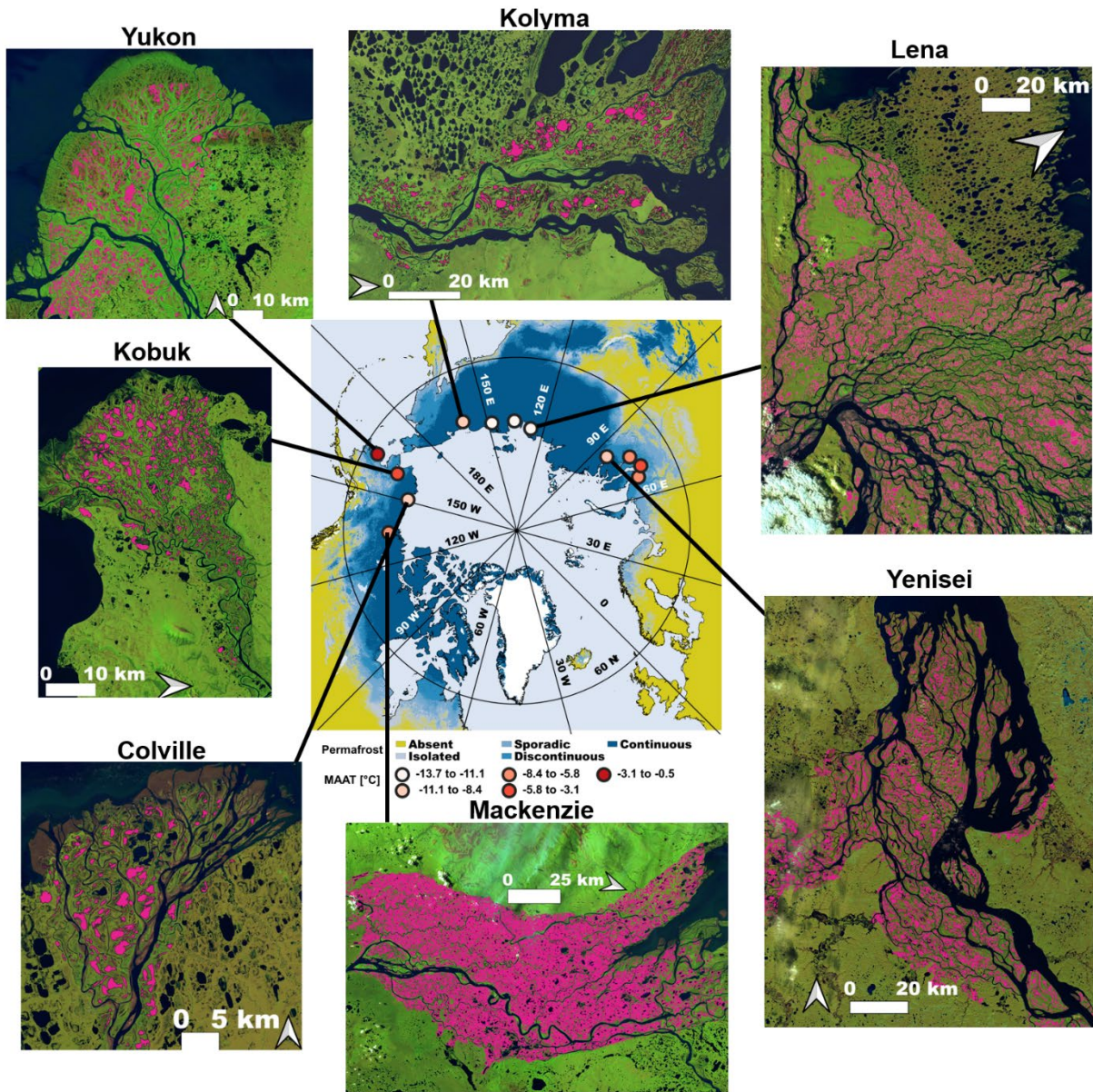
- 314 Arp, C. D., Jones, B. M., Urban, F. E., & Grosse, G. (2011). Hydrogeomorphic processes of  
315 thermokarst lakes with grounded-ice and floating-ice regimes on the Arctic coastal plain,  
316 Alaska. *Hydrological Processes*, 25(15), 2422–2438. <https://doi.org/10.1002/hyp.8019>
- 317 Bertassello, L. E., Rao, P. S. C., Jawitz, J. W., Botter, G., Le, P. V. V., Kumar, P., & Aubeneau,  
318 A. F. (2018). Wetlandscape Fractal Topography. *Geophysical Research Letters*, 45(14),  
319 6983–6991. <https://doi.org/10.1029/2018GL079094>
- 320 Bromwich, D. H., Wilson, A. B., Bai, L., Liu, Z., Barlage, M., Shih, C.-F., et al. (2017). The  
321 Arctic System Reanalysis Version 2. *Bulletin of the American Meteorological Society*,  
322 (April), BAMS-D-16-0215.1. <https://doi.org/10.1175/BAMS-D-16-0215.1>
- 323 Brown, J., Ferrians, O. J., Heginbottom, J. A., & Melnikov, E. S. (1997). *Circum-Arctic map of*  
324 *permafrost and ground-ice conditions*. Washington DC. Retrieved from  
325 <https://nsidc.org/data/ggd318>
- 326 Cael, B. B., & Seekell, D. A. (2016). The size-distribution of Earth's lakes. *Scientific Reports*,  
327 6(1), 29633. <https://doi.org/10.1038/srep29633>
- 328 Chen, M., Rowland, J. C., Wilson, C. J., Altmann, G. L., & Brumby, S. P. (2012). Temporal and  
329 spatial pattern of thermokarst lake area changes at Yukon Flats, Alaska. *Hydrological*  
330 *Processes*, 28(3), 837–852. <https://doi.org/10.1002/hyp.9642>
- 331 Chen, M., Rowland, J. C., Wilson, C. J., Altmann, G. L., & Brumby, S. P. (2013). The  
332 importance of natural variability in lake areas on the detection of permafrost degradation: A  
333 case study in the Yukon Flats, Alaska. *Permafrost and Periglacial Processes*, 24(3), 224–  
334 240. <https://doi.org/10.1002/ppp.1783>
- 335 Clauset, A., Shalizi, C. R., & Newman, M. E. J. (2009). Power-Law Distributions in Empirical  
336 Data. *SIAM Review*, 51(4), 661–703. <https://doi.org/10.1137/070710111>
- 337 Cooley, S. W., Smith, L. C., Ryan, J. C., Pitcher, L. H., & Pavelsky, T. M. (2019). Arctic-Boreal  
338 lake dynamics revealed using CubeSat imagery. *Geophysical Research Letters*, 46,  
339 2018GL081584. <https://doi.org/10.1029/2018GL081584>
- 340 Coon, E., Svyatsky, D., Jan, A., Kikinzon, E., Berndt, M., Atchley, A., et al. (2019, September).  
341 Advanced Terrestrial Simulator. <https://doi.org/10.11578/dc.20190911.1>
- 342 Crow, E. L., & Shimizu, K. (1988). *Lognormal Distributions Theory and Applications* (1st  
343 Editio). New York: Marcel Dekker.
- 344 Emmerton, C. A., Lesack, L. F. W., & Marsh, P. (2007). Lake abundance, potential water  
345 storage, and habitat distribution in the Mackenzie River Delta, western Canadian Arctic.  
346 *Water Resources Research*, 43(5), 1–14. <https://doi.org/10.1029/2006WR005139>
- 347 Engram, M., Walter Anthony, K. M., Sachs, T., Kohnert, K., Serafimovich, A., Grosse, G., &  
348 Meyer, F. J. (2020). Remote sensing northern lake methane ebullition. *Nature Climate*  
349 *Change*, 10(6), 511–517. <https://doi.org/10.1038/s41558-020-0762-8>
- 350 Gillespie, C. S. (2015). Fitting Heavy Tailed Distributions: The powerLaw Package. *Journal of*

- 351 *Statistical Software*, 64(2). <https://doi.org/10.18637/jss.v064.i02>
- 352 Grosse, G., Jones, B., & Arp, C. (2013). *Thermokarst Lakes, Drainage, and Drained Basins.*  
353 *Treatise on Geomorphology* (Vol. 8). Elsevier Ltd. [https://doi.org/10.1016/B978-0-12-](https://doi.org/10.1016/B978-0-12-374739-6.00216-5)  
354 [374739-6.00216-5](https://doi.org/10.1016/B978-0-12-374739-6.00216-5)
- 355 Hijmans, R. J. (2020). raster: Geographic Data Analysis and Modeling. Retrieved from  
356 <https://cran.r-project.org/package=raster>
- 357 van Huissteden, J., Berrittella, C., Parmentier, F. J. W., Mi, Y., Maximov, T. C., & Dolman, A. J.  
358 (2011). Methane emissions from permafrost thaw lakes limited by lake drainage. *Nature*  
359 *Climate Change*, 1(2), 119–123. <https://doi.org/10.1038/nclimate1101>
- 360 Jones, B. M., Grosse, G., Arp, C. D., Jones, M. C., Walter Anthony, K. M., & Romanovsky, V.  
361 E. (2011). Modern thermokarst lake dynamics in the continuous permafrost zone, northern  
362 Seward Peninsula, Alaska. *Journal of Geophysical Research*, 116(3), G00M03.  
363 <https://doi.org/10.1029/2011JG001666>
- 364 Jones, B. M., Arp, C. D., Grosse, G., Nitze, I., Lara, M. J., Whitman, M. S., et al. (2020).  
365 Identifying historical and future potential lake drainage events on the western Arctic coastal  
366 plain of Alaska. *Permafrost and Periglacial Processes*, 31(1), 110–127.  
367 <https://doi.org/10.1002/ppp.2038>
- 368 Kessler, M. A., Plug, L. J., & Walter Anthony, K. M. (2012). Simulating the decadal- to  
369 millennial-scale dynamics of morphology and sequestered carbon mobilization of two  
370 thermokarst lakes in NW Alaska. *Journal of Geophysical Research: Biogeosciences*,  
371 117(1), 1–22. <https://doi.org/10.1029/2011JG001796>
- 372 Le, P. V. V., & Kumar, P. (2014). Power law scaling of topographic depressions and their  
373 hydrologic connectivity. *Geophysical Research Letters*, 41(5), 1553–1559.  
374 <https://doi.org/10.1002/2013GL059114>
- 375 Lesack, L. F. W., & Marsh, P. (2010). River-to-lake connectivities, water renewal, and aquatic  
376 habitat diversity in the Mackenzie River Delta. *Water Resources Research*, 46(12), 1–16.  
377 <https://doi.org/10.1029/2010WR009607>
- 378 Lique, C., Holland, M. M., Dibike, Y. B., Lawrence, D. M., & Screen, J. A. (2016). Modeling  
379 the Arctic freshwater system and its integration in the global system: Lessons learned and  
380 future challenges. *Journal of Geophysical Research: Biogeosciences*, 121(3), 540–566.  
381 <https://doi.org/10.1002/2015JG003120>
- 382 Mandelbrot, B. B. (1982). *The Fractal Geometry of Nature* (1st ed.). New York.
- 383 Marsh, P., Lesack, L. F. W., & Roberts, A. (1999). Lake sedimentation in the Mackenzie Delta,  
384 NWT. *Hydrological Processes*, 13(16), 2519–2536. [https://doi.org/10.1002/\(SICI\)1099-](https://doi.org/10.1002/(SICI)1099-1085(199911)13:16<2519::AID-HYP935>3.0.CO;2-T)  
385 [1085\(199911\)13:16<2519::AID-HYP935>3.0.CO;2-T](https://doi.org/10.1002/(SICI)1099-1085(199911)13:16<2519::AID-HYP935>3.0.CO;2-T)
- 386 Mitzenmacher, M. (2004). A Brief History of Generative Models for Power Law and Lognormal  
387 Distributions. *Internet Mathematics*, 1(2), 226–251.  
388 <https://doi.org/10.1080/15427951.2004.10129088>
- 389 Muster, S., Riley, W. J., Roth, K., Langer, M., Cresto Aleina, F., Koven, C. D., et al. (2019). Size

- 390 Distributions of Arctic Waterbodies Reveal Consistent Relations in Their Statistical  
391 Moments in Space and Time. *Frontiers in Earth Science*, 7(January), 1–15.  
392 <https://doi.org/10.3389/feart.2019.00005>
- 393 Nienhuis, J. H., Ashton, A. D., & Giosan, L. (2016). Littoral steering of deltaic channels. *Earth*  
394 *and Planetary Science Letters*, 453(April 2018), 204–214.  
395 <https://doi.org/10.1016/j.epsl.2016.08.018>
- 396 Nienhuis, J. H., Hoitink, A. J. F. T., & Törnqvist, T. E. (2018). Future Change to Tide-Influenced  
397 Deltas. *Geophysical Research Letters*, 45(8), 3499–3507.  
398 <https://doi.org/10.1029/2018GL077638>
- 399 Nienhuis, J. H., Ashton, A. D., Edmonds, D. A., Hoitink, A. J. F., Kettner, A. J., Rowland, J. C.,  
400 & Törnqvist, T. E. (2020). Global-scale human impact on delta morphology has led to net  
401 land area gain. *Nature*, 577(7791), 514–518. <https://doi.org/10.1038/s41586-019-1905-9>
- 402 Nitze, I., Grosse, G., Jones, B. M., Romanovsky, V. E., & Boike, J. (2018). Remote sensing  
403 quantifies widespread abundance of permafrost region disturbances across the Arctic and  
404 Subarctic. *Nature Communications*, 9(1), 5423. [https://doi.org/10.1038/s41467-018-07663-](https://doi.org/10.1038/s41467-018-07663-3)  
405 3
- 406 Obu, J., Westermann, S., Bartsch, A., Berdnikov, N., Christiansen, H. H., Dashtseren, A., et al.  
407 (2019). Northern Hemisphere permafrost map based on TTOP modelling for 2000–2016 at  
408 1 km<sup>2</sup> scale. *Earth-Science Reviews*, 193(October 2018), 299–316.  
409 <https://doi.org/10.1016/j.earscirev.2019.04.023>
- 410 Overeem, I., Jafarov, E., Wang, K., Schaefer, K., Stewart, S., Clow, G., et al. (2018). A  
411 Modeling Toolbox for Permafrost Landscapes. *Eos*, 99.  
412 <https://doi.org/10.1029/2018EO105155>
- 413 Pau, G., Fuchs, F., Sklyar, O., Boutros, M., & Huber, W. (2010). EBImage-an R package for  
414 image processing with applications to cellular phenotypes. *Bioinformatics*, 26(7), 979–981.  
415 <https://doi.org/10.1093/bioinformatics/btq046>
- 416 Pebesma, E. (2018). Simple Features for R: Standardized Support for Spatial Vector Data. *The R*  
417 *Journal*, 10(1), 439. <https://doi.org/10.32614/RJ-2018-009>
- 418 Pebesma, E. (2020). stars: Spatiotemporal Arrays, Raster and Vector Data Cubes. Retrieved from  
419 <https://cran.r-project.org/package=stars>
- 420 Pekel, J.-F., Cottam, A., Gorelick, N., & Belward, A. S. (2016). High-resolution mapping of  
421 global surface water and its long-term changes. *Nature*, 540(7633), 418–422.  
422 <https://doi.org/10.1038/nature20584>
- 423 Petrescu, A. M. R., Van Beek, L. P. H., Van Huissteden, J., Prigent, C., Sachs, T., Corradi, C. A.  
424 R., et al. (2010). Modeling regional to global CH<sub>4</sub> emissions of boreal and arctic wetlands.  
425 *Global Biogeochemical Cycles*, 24(4), 1–12. <https://doi.org/10.1029/2009GB003610>
- 426 Piliouras, A., & Rowland, J. C. (2020). Arctic River Delta Morphologic Variability and  
427 Implications for Riverine Fluxes to the Coast. *Journal of Geophysical Research: Earth*  
428 *Surface*, 125(1), 1–20. <https://doi.org/10.1029/2019JF005250>

- 429 Piliouras, A., Lauzon, R., & Rowland, J. C. (2021). Unraveling the Combined Effects of Ice and  
430 Permafrost on Arctic Delta Morphodynamics. *Journal of Geophysical Research: Earth*  
431 *Surface*, 126(4), 1–17. <https://doi.org/10.1029/2020JF005706>
- 432 Plug, L. J., & West, J. J. (2009). Thaw lake expansion in a two-dimensional coupled model of  
433 heat transfer, thaw subsidence, and mass movement. *Journal of Geophysical Research*,  
434 114(F1), F01002. <https://doi.org/10.1029/2006JF000740>
- 435 Plug, L. J., Walls, C., & Scott, B. M. (2008). Tundra lake changes from 1978 to 2001 on the  
436 Tuktoyaktuk Peninsula, western Canadian Arctic. *Geophysical Research Letters*, 35(3),  
437 L03502. <https://doi.org/10.1029/2007GL032303>
- 438 Rey, D. M., Walvoord, M., Minsley, B., Rover, J., & Singha, K. (2019). Investigating lake-area  
439 dynamics across a permafrost-thaw spectrum using airborne electromagnetic surveys and  
440 remote sensing time-series data in Yukon Flats, Alaska. *Environmental Research Letters*,  
441 14(2), 025001. <https://doi.org/10.1088/1748-9326/aaf06f>
- 442 Rowland, J. C., Jones, C. E., Altmann, G., Bryan, R., Crosby, B. T., Geernaert, G. L., et al.  
443 (2010). Arctic landscapes in transition: Responses to thawing permafrost. *Eos*, 91(26), 229–  
444 230. <https://doi.org/10.1029/2010EO260001>
- 445 Rowland, J. C., Travis, B. J., & Wilson, C. J. (2011). The role of advective heat transport in talik  
446 development beneath lakes and ponds in discontinuous permafrost. *Geophysical Research*  
447 *Letters*, 38(17), 1–5. <https://doi.org/10.1029/2011GL048497>
- 448 Schuur, E. A. G., McGuire, A. D., Schädel, C., Grosse, G., Harden, J. W., Hayes, D. J., et al.  
449 (2015). Climate change and the permafrost carbon feedback. *Nature*, 520(7546), 171–179.  
450 <https://doi.org/10.1038/nature14338>
- 451 Smith, L. C., Sheng, Y., MacDonald, G. M., & Hinzman, L. D. (2005). Disappearing Arctic  
452 Lakes. *Science*, 308(5727), 1429–1429. <https://doi.org/10.1126/science.1108142>
- 453 Squires, M. M., Lesack, L. F. W., Hecky, R. E., Guildford, S. J., Ramlal, P., & Higgins, S. N.  
454 (2009). Primary production and carbon dioxide metabolic balance of a lake-rich arctic river  
455 floodplain: Partitioning of phytoplankton, epipelon, macrophyte, and epiphyton production  
456 among lakes on the mackenzie delta. *Ecosystems*, 12(5), 853–872.  
457 <https://doi.org/10.1007/s10021-009-9263-3>
- 458 Syvitski, J. P. M., Kettner, A. J., Overeem, I., Hutton, E. W. H., Hannon, M. T., Brakenridge, G.  
459 R., et al. (2009). Sinking deltas due to human activities. *Nature Geoscience*, 2(10), 681–  
460 686. <https://doi.org/10.1038/ngeo629>
- 461 Tank, S. E., Lesack, L. F. W., & Hesslein, R. H. (2009). Northern Delta lakes as summertime  
462 CO<sub>2</sub> absorbers within the arctic landscape. *Ecosystems*, 12(1), 144–157.  
463 <https://doi.org/10.1007/s10021-008-9213-5>
- 464 Tejedor, A., Longjas, A., Zaliapin, I., & Foufoula-Georgiou, E. (2015a). Delta channel networks:  
465 1. A graph-theoretic approach for studying connectivity and steady state transport on deltaic  
466 surfaces. *Water Resources Research*, 51(6), 3998–4018.  
467 <https://doi.org/10.1002/2014WR016577>
- 468 Tejedor, A., Longjas, A., Zaliapin, I., & Foufoula-Georgiou, E. (2015b). Delta channel networks:

- 469 2. Metrics of topologic and dynamic complexity for delta comparison, physical inference,  
470 and vulnerability assessment. *Water Resources Research*, 51(6), 4019–4045.  
471 <https://doi.org/10.1002/2014WR016604>
- 472 Tejedor, A., Longjas, A., Caldwell, R., Edmonds, D. A., Zaliapin, I., & Foufoula-Georgiou, E.  
473 (2016). Quantifying the signature of sediment composition on the topologic and dynamic  
474 complexity of river delta channel networks and inferences toward delta classification.  
475 *Geophysical Research Letters*, 43(7), 3280–3287. <https://doi.org/10.1002/2016GL068210>
- 476 Tejedor, A., Longjas, A., Edmonds, D. A., Zaliapin, I., Georgiou, T. T., Rinaldo, A., &  
477 Foufoula-Georgiou, E. (2017). Entropy and optimality in river deltas. *Proceedings of the*  
478 *National Academy of Sciences*, 114(44), 11651–11656.  
479 <https://doi.org/10.1073/pnas.1708404114>
- 480 Victorov, A. S., Orlov, T. V., Kapralova, V. N., Trapeznikova, O. N., Sadkov, S. A., & Zverev,  
481 A. V. (2019). Stochastic Modeling of Natural Lacustrine Thermokarst Under Stable and  
482 Unstable Climate. In *Natural Hazards and Risk Research in Russia* (pp. 241–267).  
483 [https://doi.org/10.1007/978-3-319-91833-4\\_18](https://doi.org/10.1007/978-3-319-91833-4_18)
- 484 Vulis, L., Tejedor, A., Schwenk, J., Piliouras, A., Rowland, J., & Foufoula-Georgiou, E. (2020).  
485 Channel Network Control on Seasonal Lake Area Dynamics in Arctic Deltas. *Geophysical*  
486 *Research Letters*, 47(7). <https://doi.org/10.1029/2019GL086710>
- 487 Walker, H. J. (1998). Arctic Deltas. *Journal of Coastal Research*, 14(3), 719–738. Retrieved  
488 from <http://www.jstor.org/stable/4298831>
- 489 Walvoord, M. A., & Kurylyk, B. L. (2016). Hydrologic Impacts of Thawing Permafrost-A  
490 Review. *Vadose Zone Journal*, 15(6), 1–20. <https://doi.org/10.2136/vzj2016.01.0010>
- 491 Yoshikawa, K., & Hinzman, L. D. (2003). Shrinking thermokarst ponds and groundwater  
492 dynamics in discontinuous permafrost near Council, Alaska. *Permafrost and Periglacial*  
493 *Processes*, 14(2), 151–160. <https://doi.org/10.1002/ppp.451>
- 494
- 495

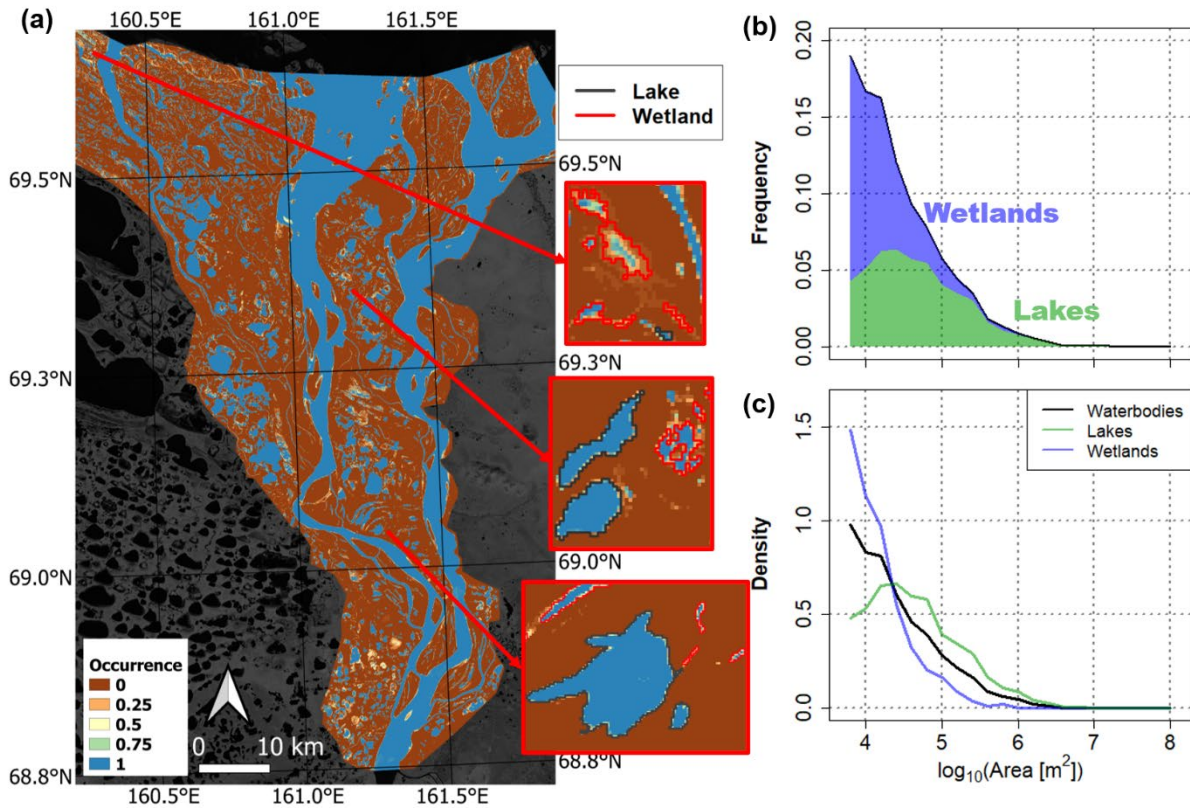


496

497 **Figure 1. Arctic deltas examined in this study.** Twelve arctic deltas (see colored open circles in the central panel  
 498 for location) were examined along a range of Mean Annual Air Temperature (MAAT) and ice content. The central  
 499 map shows delta locations, colored by 2000-2016 mean MAAT, estimated from the Arctic Systems Reanalysis V2  
 500 (Bromwich et al., 2017), and underlain by Arctic permafrost zonation (Obu et al., 2019). Summertime Landsat-8  
 501 scenes of 7 out of the 12 delta are shown with waterbodies identified from a single July Global Surface Water mask  
 502 (Pekel et al., 2016) colored in pink.

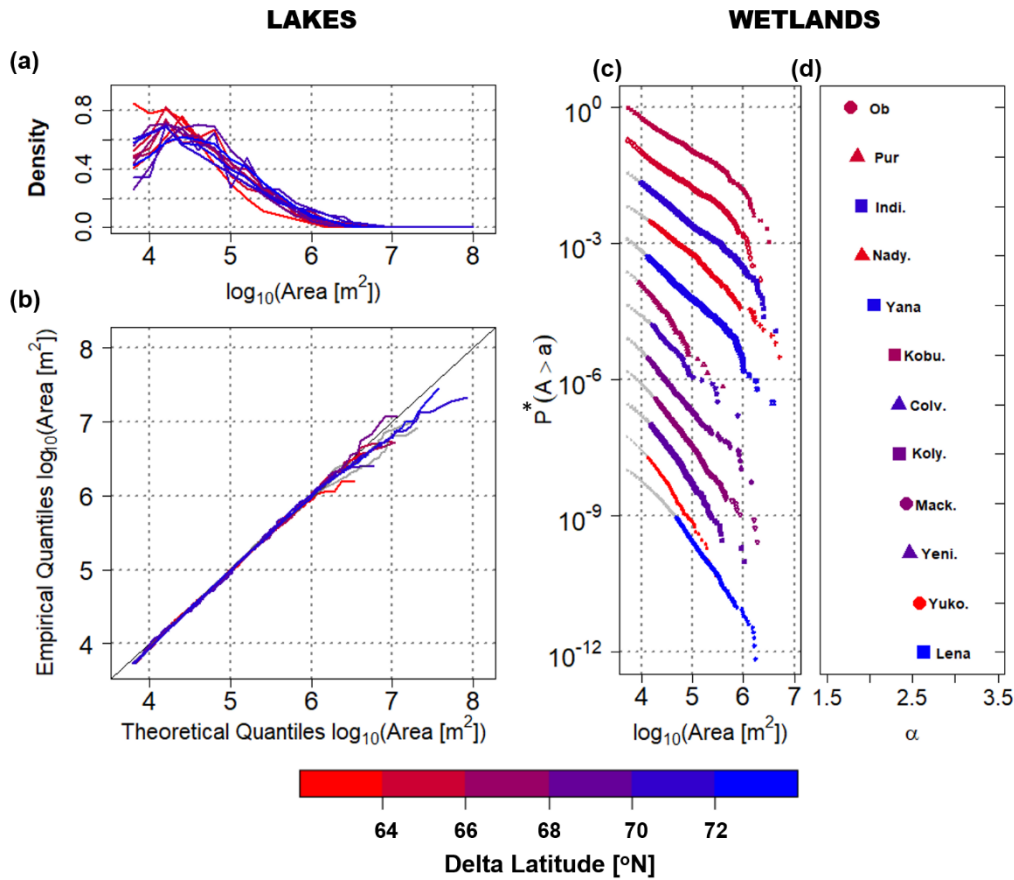
503

504

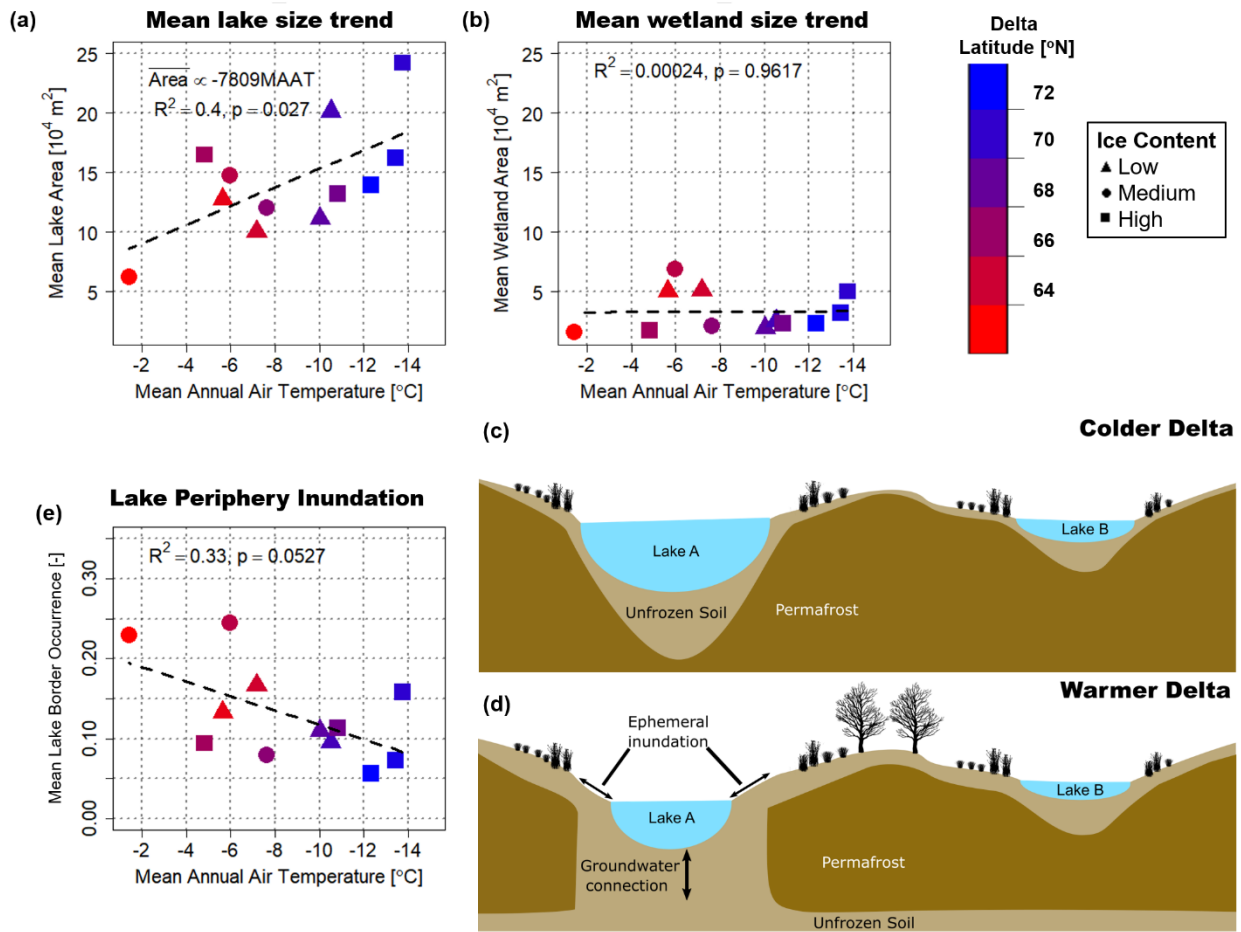


505  
506

507 **Figure 2. Example of waterbody classification procedure on Kolyma Delta.** The waterbody classification  
 508 procedure which marks waterbodies as either perennial lakes or ephemeral wetlands based on their July occurrence  
 509 index, and the resulting size distribution. (a) July pixel water occurrence  $w_i$  over the Kolyma delta from 1999 to 2018.  
 510 Brown indicates land pixels ( $w_i = 0$ ) and blue indicates perennially inundated water pixels ( $w_i = 1$ ), with colors in  
 511 between indicating water pixels indicated only a fraction of the time. (b) The histogram of waterbody sizes is  
 512 partitioned into the relative fraction of lakes (green) and wetlands (blue) at an occurrence index threshold  $\theta = 0.85$ .  
 513 (c) The probability density function (PDF) of lake sizes in green and wetland sizes in blue, compared with waterbody  
 514 sizes in black.



515 **Figure 3. Size distributions of lakes and wetlands extracted at occurrence index threshold  $\theta = 0.85$ .** (a) Lake  
 516 size PDFs for the 12 deltas, (b) quantile-quantile plots of the lognormal with truncation from below at the minimum  
 517 lake size (5,400 m<sup>2</sup>) fitted to the lake size distribution. In (b) fitted distributions whose fit to data is rejected at the 5%  
 518 significance level (KS test) are in grey. (c) Wetland size exceedance probability, (d) fitted power law exponent,  $\alpha$ , of  
 519 all 12 deltas. The exceedance probabilities in (c) are rescaled by a factor  $\tau$ , i.e.  $P^* = P\tau$ , for visual display, and are  
 520 ordered by increasing values of  $\alpha$  to highlight the range of observed  $\alpha$ . For each delta, power laws are fit to the colored  
 521 points above the minimum wetland size,  $x_0$ , which was optimally determined using the procedure of Clauset et al.  
 522 (2009). The power law parameter  $\alpha$  in (d) is the scaling exponent of the PDF.  
 523



524

525 **Figure 4. Lake and wetland size climate trends.** (a) Scatterplot between mean lake size and MAAT showing a  
 526 significant relationship between the two. (b) Scatterplot between mean wetland size and MAAT showing lack of a  
 527 significant relationship. (c, d) The relationship between lake size and MAAT is attributed to colder deltas having  
 528 thicker permafrost which prevents lakes from connecting to the sub-permafrost aquifer. In warmer deltas, connection  
 529 to the sub-permafrost aquifer leads to greater lake level change over the summer, driving increased variability in  
 530 inundation along the peripheries of lakes, and diminishing rates of thermally-driven lateral expansion. (e) Scatterplot  
 531 between the fraction of the periphery of large lakes that remains water on average over the period of record and MAAT  
 532 shows a weak (i.e.  $p \sim 0.05$ ) linear relationship, supporting this mechanism.